

In silico molecular docking and molecular dynamics of *Prinsepia utilis* phytochemicals as potential inhibitors of phosphodiesterase 4B

Journal of Chemical Research
November-December 1–13
© The Author(s) 2024
Article reuse guidelines:
sagepub.com/journals-permissions
DOI: 10.1177/17475198241305879
journals.sagepub.com/home/chl



Cao Hoang Minh Chau¹, Ngu Thi Tra Giang¹, Nguyen Thi Thuy Tram¹,
Le Thi My Chau², Nguyen Xuan Ha³  and Phan Thi Thuy¹ 

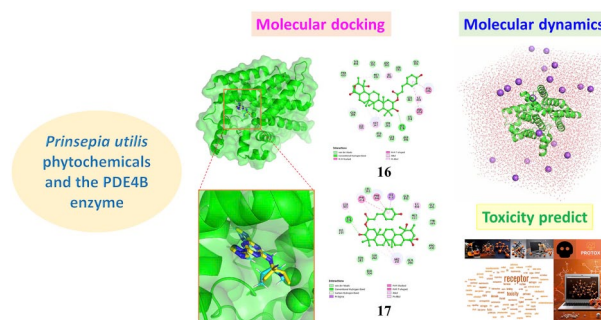
Abstract

Phosphodiesterase 4B is an important enzyme belonging to the phosphodiesterase family, playing a role in regulating the levels of cyclic AMP in cells. Phosphodiesterase 4B degrades cyclic AMP, a crucial signaling molecule involved in numerous biological processes, including inflammation regulation. Recently, the search for potential inhibitors with fewer side effects and high biological activity in valuable medicinal plants has drawn the attention of current scientists. Various *in silico* methods have been applied to reduce costs and time for experimental studies. In this study, an *in silico* screening involving a set of 131 natural compounds sourced from *Prinsepia utilis* species was conducted. These compounds were docked into the active site of the phosphodiesterase 4B protein. As a result, 10 compounds exhibited the most potential inhibitory activity against phosphodiesterase 4B, including 2 α -O-trans-*p*-coumaroyl-3 β ,19 α -dihydroxy-urs-12-en-28-oic acid, 2 α -O-cis-*p*-coumaroyl-3 β ,19 α -dihydroxy-urs-12-en-28-oic acid, cyanidin-3-O-rutinoside, delphinidin-3-O-rutinoside, peonidin-3-O-rutinoside, rutin, isorhamnetin-3-O-rutinoside, kaempferol 3-O- α -L-rhamnopyranosyl-(1 \rightarrow 6)- β -D-glucopyranoside-7-O- β -D-glucopyranoside, kaempferol 3-O- α -L-rhamnopyranosyl-(1 \rightarrow 6) [α -L-rhamnopyranosyl-(1 \rightarrow 2)]- β -D-glucopyranoside, quercetin 3-O- α -L-rhamnopyranosyl-(1 \rightarrow 6)- β -D-glucopyranoside were identified through molecular docking simulations. Subsequently, molecular dynamics simulations were performed on these complexes, revealing significant findings regarding their stability. Furthermore, MM-GBSA calculations indicated that the potential compounds had stronger binding free energies than the reference inhibitor. Finally, the selected compounds were subjected to toxicity prediction, showing noteworthy results with large LD₅₀ values and safe toxicity levels. Therefore, these compounds could be potential candidates for further experimental studies as phosphodiesterase 4B inhibitors.

Keywords

Molecular Dynamics, MM-GBSA, molecular docking, phosphodiesterase 4B (PDE4B), *Prinsepia utilis*, toxicity

Date received: 13 June 2024; accepted: 22 November 2024



¹Department of Chemistry, Vinh University, Vinh City, Nghean, Vietnam

²School of Biochemical and Environmental Technology, Vinh University, Vinh City, Nghean, Vietnam

³Institute of Natural Products Chemistry, Vietnam Academy of Science and Technology, Cau Giay, Hanoi, Vietnam

Corresponding authors:

Nguyen Xuan Ha, Institute of Natural Products Chemistry, Vietnam Academy of Science and Technology, 18 Hoang Quoc Viet, Cau Giay 122100, Hanoi, Vietnam.
Email: hanguyenxuan98@gmail.com

Phan Thi Thuy, Department of Chemistry, Vinh University, 182 Le Duan, Vinh 43000, Nghe An, Viet Nam.
Emails: thuypt@vinhuni.edu.vn; phanthuyhtc@gmail.com



Introduction

Inflammation is a multifaceted process that is often studied from various angles, with infectious and autoimmune inflammations being the most researched. It can occur in different parts of the body and lead to serious health issues.¹ One enzyme of interest in the context of inflammation is phosphodiesterase 4B (PDE4B). PDE4B, a member of the phosphodiesterase (PDE) family, degrades cyclic nucleotides such as cAMP and cGMP, thus reducing these crucial second messenger signals within cells. cAMP is renowned for its anti-inflammatory properties and is widely used in pharmacology to treat inflammatory diseases.^{2,3} Recent studies have identified cAMP as a key coordinator in resolving inflammation.⁴ In addition, cAMP regulates cellular metabolism by activating protein kinase A (PKA) and targeting proteins directly activated by cAMP, impacting numerous essential cellular functions across all cell types. Research has shown that knocking down PDE4B effectively inhibits lipopolysaccharide (LPS)-induced activation of NF- κ B and inflammatory responses in various cell types. Deleting PDE4B also reduces the LPS-induced production of reactive oxygen species (ROS).⁴ PDE4B plays a role in releasing inflammatory mediators from immune cells, thereby amplifying the inflammatory response. Therefore, inhibiting PDE4B activity could be a potential strategy for controlling inflammation. Recently, the application of molecular docking and molecular dynamics (MD) simulations in discovering PDE4B inhibitors has shown considerable success.⁵⁻⁷

Prinsepia utilis Royle, a member of the *Prinsepia* genus within the Rosaceae family, holds significant medicinal value and is often widely used in traditional medicine for treating various ailments like joint pain and inflammation.⁸ So far, around 131 compounds have been identified from different parts of *P. utilis*, spanning terpenoids, flavonoids, lignans, and sterols.⁹⁻¹¹ Alongside chemical exploration, researchers have focused on assessing its diverse biological activities, including antioxidant, hypoglycemic, α -glucosidase inhibitory, cytotoxic, anti-inflammatory, immunosuppressive, antibacterial, and lipase inhibitory properties.⁹ Particularly noteworthy are its potential anti-inflammatory effects. Thakur et al. conducted an *in vivo* study on the methanolic extract of *P. utilis* flowers using a rat pedal edema model induced by carrageenan. The results revealed significant anti-inflammatory activity at both 100 mg/kg body weight (64.38% inhibition) and 200 mg/kg body weight (65.75% inhibition).¹² *P. utilis* seed oil has shown promise as a natural anti-inflammatory and analgesic, evident from *in vitro* trypsin inhibition assays and serum bovine albumin denaturation tests. These tests demonstrated a dose-dependent response with IC₅₀ values of 63.57 and 518.14 μ g/mL, respectively. Moreover, *in vivo* experiments showcased effective anti-inflammatory activity, with significant inhibition lasting up to 4 h against carrageenan- and formalin-induced mouse paw edema at a maximum experimental dose of 200 mg/kg body weight.¹³ In addition, *P. utilis* water extract exhibited inhibitory effects on allergic contact dermatitis symptoms in mice induced by fluorescein

isothiocyanate (FITC), by repairing tissue barriers and reducing Th2-type allergic inflammation.¹⁴

Despite these promising findings, information regarding the anti-inflammatory properties of this species remains limited. Hence, current research endeavors have undertaken *in silico* studies on compounds from *P. utilis* to aid in the discovery of phosphodiesterase-4 inhibitory agents for treating inflammatory diseases.

Materials and methods

Molecular docking

The chemical structures of all compounds derived from *P. utilis* were drawn using Marvin JS software and then energy-minimized in the Avogadro software with the MMFF94s force field.^{9,15} The chemical structures of the ligands were further converted to PDBQT format using AutoDockTools software. The crystal structure of the human phosphodiesterase 4B (PDE4B) protein was downloaded from the RCSB Protein Data Bank (<https://www.rcsb.org/structure/4KP6>) with PDB ID: 4KP6 and a resolution of 1.50 Å.¹⁶ The protein molecules were prepared before docking using Chimera and AutoDockTools software. The preparation process involved removing water molecules and co-crystallized ligands, then adding polar hydrogens, Kollman partial charges, and converting to PDBQT format. AutoDock Vina was used for docking the molecules between the ligand structure and the target protein.^{17,18} A grid box was selected to cover the binding site of the co-crystallized ligand at the center coordinates $x=-41.8$ Å, $y=91.2$ Å, $z=114.4$ Å, the box size of $24 \times 24 \times 24$, and the spacing of 1. All parameters during the docking experiment were set to default, except for the exhaustiveness value which was set to 400. The protocol validation for this docking process was conducted through re-docking. PyMOL and Discovery Studio Visualizer software were used to visualize the interaction modes of ligand-protein.

Molecular dynamics (MD)

To monitor the movement of each atom in a system over time and have information about their relative positions, MD simulations were applied using the GROMACS v2023.1 software package.¹⁹ The AMBER99SB-ILDN force field was used to parameterize the protein PDE4B (PDB ID: 4KP6). The energy of the docked ligand structure was calculated using the B3LYP/6-31G** function set with the Gaussian09 program, followed by generating ligand topology parameters through a combination of the GAFF and GLYCAM_06j-1 force fields, utilizing ACPYPE and AmberTools 22.^{20,21} The protein-ligand complex system was solvated with the TIP3P water model placed in a triclinic box and neutralized by adding counter ions (Na⁺). To ensure system stability, the steepest descent algorithm was used for energy minimization with a maximum force of 1000 kJ.mol⁻¹.nm⁻¹ and performed with 50,000 steps. Then, the systems were equilibrated through two steps: the NVT ensemble and the NPT ensemble at 100 ps to maintain the temperature and pressure at 310 K and 1 atm. The production MD were run for 200 ns to relax the system,

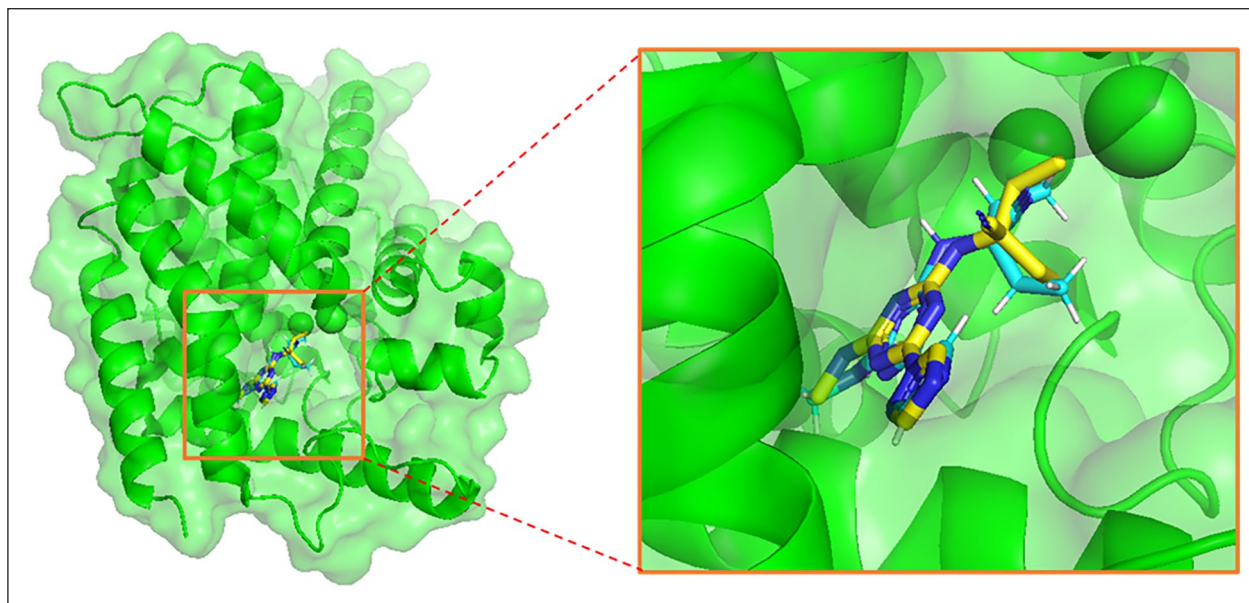


Figure 1. Superimposition of the co-crystallized ligand (cyan) and the redocked ligand (yellow) in the PDE4B protein with an RMSD value of 1.25556 Å.

and trajectories were saved every 2.0 ps. Post-simulation analyses including RMSD and RMSF were plotted using the Matplotlib tool in Python.

MM–GBSA calculations

The binding free energy of the protein complex system in a 200 ns MD simulation was estimated using the `gmx_MMPBSA v1.4.3` program, employing the MM/GBSA

$$\Delta G_{\text{bind}} = G_{\text{complex}} - G_{\text{receptor}} - G_{\text{ligand}} = \Delta H - T\Delta S = \Delta E_{\text{MM}} + \Delta G_{\text{sol}} - T\Delta S$$

Here, $\Delta E_{\text{MM}} = \Delta E_{\text{covalent}} + \Delta E_{\text{ele}} + \Delta E_{\text{vdW}} = (\Delta E_{\text{bond}} + \Delta E_{\text{angle}} + \Delta E_{\text{dihedral}}) + \Delta E_{\text{ele}} + \Delta E_{\text{vdW}}$ and $\Delta G_{\text{sol}} = \Delta G_{\text{GB}} + \Delta G_{\text{SA}}$.

In this context, G_{complex} is the Gibbs free energy of the PDE4B complex with the studied compound, G_{receptor} is the Gibbs free energy of the PDE4B protein, and G_{ligand} is the Gibbs free energy of the unbound studied compound. ΔH represents the enthalpy of binding, while $-T\Delta S$ corresponds to the entropy changes upon ligand binding. ΔE_{MM} (or ΔG_{Gas}) denotes the change in molecular mechanic energy in the gas phase, encompassing changes in internal energy ΔE_{int} (bond, angle, and dihedral energies), electrostatic energy ΔE_{ele} , and van der Waals energy ΔE_{vdW} . The solvation free energy ΔG_{so} includes the polar contribution (electrostatic solvation energy calculated via the GB model) and the nonpolar contribution ΔE_{surf} or ΔG_{SA} (estimated using the solvent-accessible surface area) between the solute and the continuum solvent.^{22,23}

Toxicity prediction

ProTox 3.0 (<https://tox-new.charite.de/protox3/>) is a powerful and efficient tool for predicting the toxicity of potential compounds. Utilizing this tool not only saves time and costs but also enhances accuracy and efficiency in toxicity

(Molecular Mechanics/Generalized Born Surface Area) approach.²² These calculations were performed using the single trajectory (ST) method, with the AMBERFF99SB-ILDN and GAFF2 force fields applied to the protein and ligand, respectively. A total of 20,000 snapshots from each 200 ns MD simulation trajectory were utilized for the binding free energy calculations. The MM/GBSA binding energy was determined by summing the contributions of various interactions, represented as follows

research. This significantly contributes to the development of safe and effective compounds in the pharmaceutical and chemical fields.²⁴ Therefore, ProTox 3.0 online tools were employed to study the toxicity properties of the selected compounds for the current research.

Results

Molecular docking

Molecular docking simulation is an important computational method in the search for potential inhibitors from screening natural compound datasets of medicinal plant species.^{25,26} In this study, a database of compounds sourced from *P. utilis* was subjected to molecular docking against the target protein PDE4B (PDB ID: 4KP6). Before docking, protocol confirmation is necessary through the redocking process. The obtained results are presented in Figure 1, where the overlaid ligand after redocking with the initial ligand shows deviation within an acceptable range as the calculated RMSD value is 1.25556 Å ($<2\text{Å}$).^{27,28} The redocked ligand 2-ethyl-2-[[4-(methylamino)-6-(1H-1,2,4-triazol-1-yl)-1,3,5-triazin-2-yl]amino]butanenitrile (1S1), a known PDE-4B inhibitor with an experimental *in vitro* IC_{50} value of 0.81 nM, was chosen as the positive control in

Table 1. The binding affinities of the top-hit compounds and their interactions with the PDE4B protein.

ID	Compound	Binding affinity (kcal/mol)	Amino acid residues in contacts	Interaction type	No. of hydrogen bonds
16	2 α -O-Trans-p-coumaroyl-3 β ,19 α -dihydroxy-urs-12-en-28-oic acid	-10.81	His278 Leu303, Met347, Ile410, Ile450 Phe414, Phe446	Hydrogen bond Alkyl and π -alkyl π - π T-shaped and π - π stacked	1
17	2 α -O-Cis-p-coumaroyl-3 β ,19 α -dihydroxy-urs-12-en-28-oic acid	-10.74	His278 Leu303, Ile450, Met347 Ile410 His234 Phe414, Phe446	Hydrogen bond Alkyl and π -alkyl π - σ Carbon hydrogen bond π - π T-shaped and π - π stacked	1
40	Cyanidin-3-O-rutinoside	-10.29	Tyr233, Asn283, His278, Thr345, His234 Ile410, Met347 Phe414, Phe446, His234	Hydrogen bond Alkyl and π -alkyl π - π T-shaped and π - π stacked	5
42	Delphinidin-3-O-rutinoside	-10.24	Asn395, Met347, Glu304 Ile410 Phe446, Tyr233	Hydrogen bond π -alkyl π - π T-shaped, π - π staked	3
44	Peonidin-3-O-rutinoside	-11.22	Gln443, Asn395, Asp392, His278, Asp275, Asp346, Asn283 Ile410 Phe446	Hydrogen bond π -alkyl π - π stacked	7
50	Rutin	-10.52	His278, Asp392, Asn283, Asp346, Gln443 Ile410 Phe446, Tyr233	Hydrogen bond π -alkyl π - π T-shaped, π - π staked	5
53	Isorhamnetin-3-O-rutinoside	-10.24	Asn395, Asp346, Asn283, Asp275, Asp392, His278 Met347, Ile410 Phe446	Hydrogen bond π -alkyl π - π staked	6
68	Kaempferol 3-O- α -L-rhamnopyranosyl- (1 \rightarrow 6)- β -D- glucopyranoside-7-O- β -D-glucopyranoside	-10.20	Asp346, Asn283, Gln284, Ser282, Pro430 Tyr233, Phe446, Phe414 Ile410 Met347, Met431 His234	Hydrogen bond π - π T-shaped, π - π staked π - σ , π -alkyl π -sulfur Carbon hydrogen bond	5
70	Kaempferol 3-O- α -L-rhamnopyranosyl- (1 \rightarrow 6) [α -L- rhamnopyranosyl- (1 \rightarrow 2)]- β -D- glucopyranoside	-10.13	Thr345, Glu304 Met347, Ile410 Phe446, Tyr233	Hydrogen bond Alkyl and π -alkyl π - π T-shaped, π - π staked	2
72	Quercetin 3-O- α -L-rhamnopyranosyl- (1 \rightarrow 6)- β -D- glucopyranoside	-10.10	Glu304, Asn283, Asn395, Thr345, Asp392 Ile410, Met347 Phe446 Asp392 Ser282	Hydrogen bond π -alkyl π - π staked π -anion Carbon hydrogen bond	5

this study.¹⁶ After successful protocol confirmation, the compounds were docked, and the results are presented in Tables 1 and Supplemental Table S1. It can be observed that the binding affinities of the studied compounds range from -1.55 to -11.22 kcal/mol, whereas the control compound 1S1 has an affinity of -7.25 kcal/mol. As observed in Supplemental Table S1, the top 10 potential compounds exhibited affinities lower than -10 kcal/mol. These compounds were selected for further analysis of their interaction mode and binding capability with the target protein PDE4B as presented in Table 1 and Figure 2.

Five natural rutinosides—specifically cyanidin-3-O-rutinoside (compound 40), delphinidin-3-O-rutinoside (compound 42), peonidin-3-O-rutinoside (compound 44), rutin (compound 50), and isorhamnetin-3-O-rutinoside (compound 53)—demonstrate strong binding affinities with ΔG values of -10.29, -10.24, -11.22, -10.52, and -10.24 kcal/mol, respectively. Among these, compound 44 forms the highest number of hydrogen bonds with seven amino acid residues—Gln443, Asn395, Asp392, His278, Asp275, Asp346, and Asn283—resulting in the strongest binding affinity ($\Delta G = -11.22$ kcal/mol). The predominance of

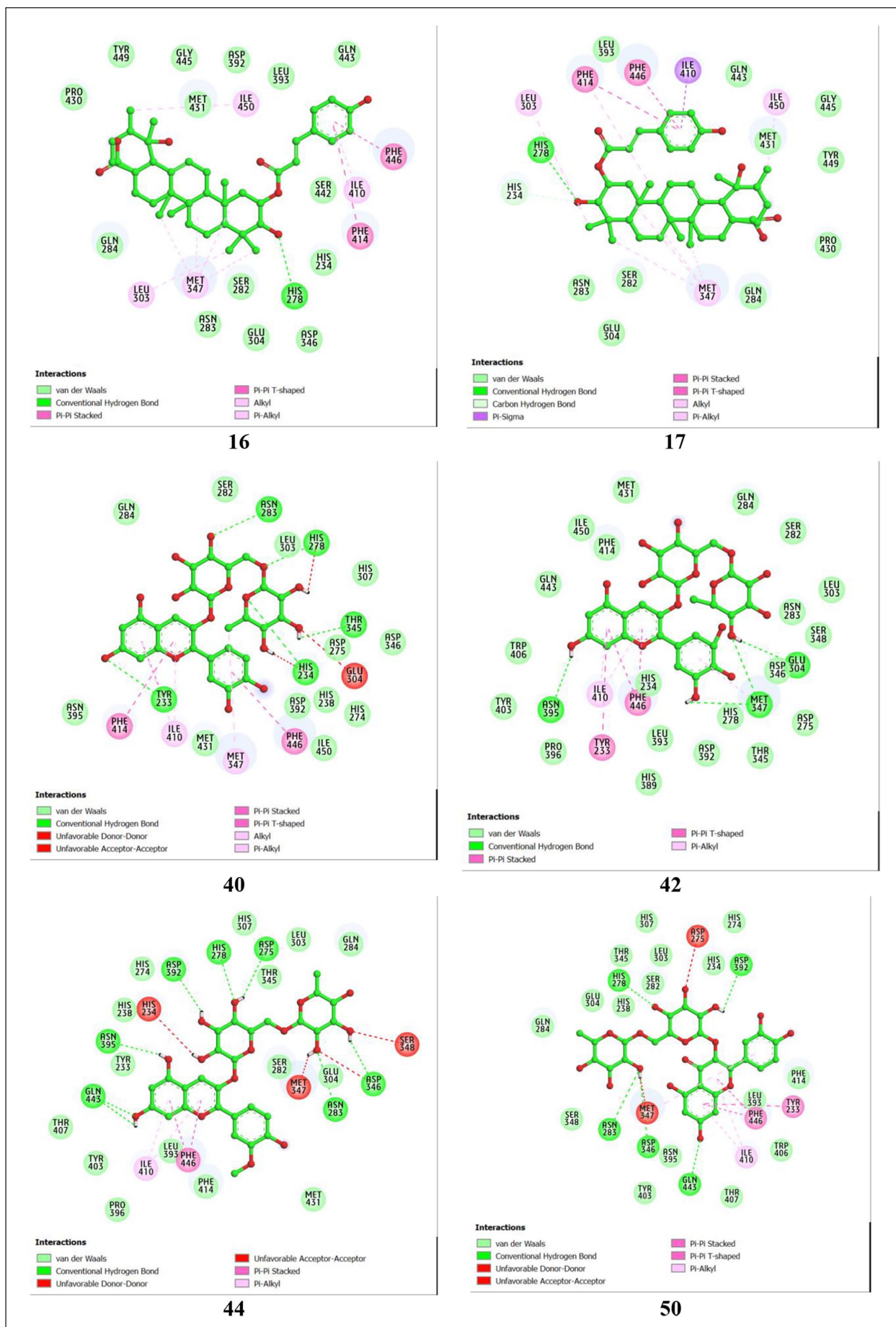


Figure 2. (Continued)

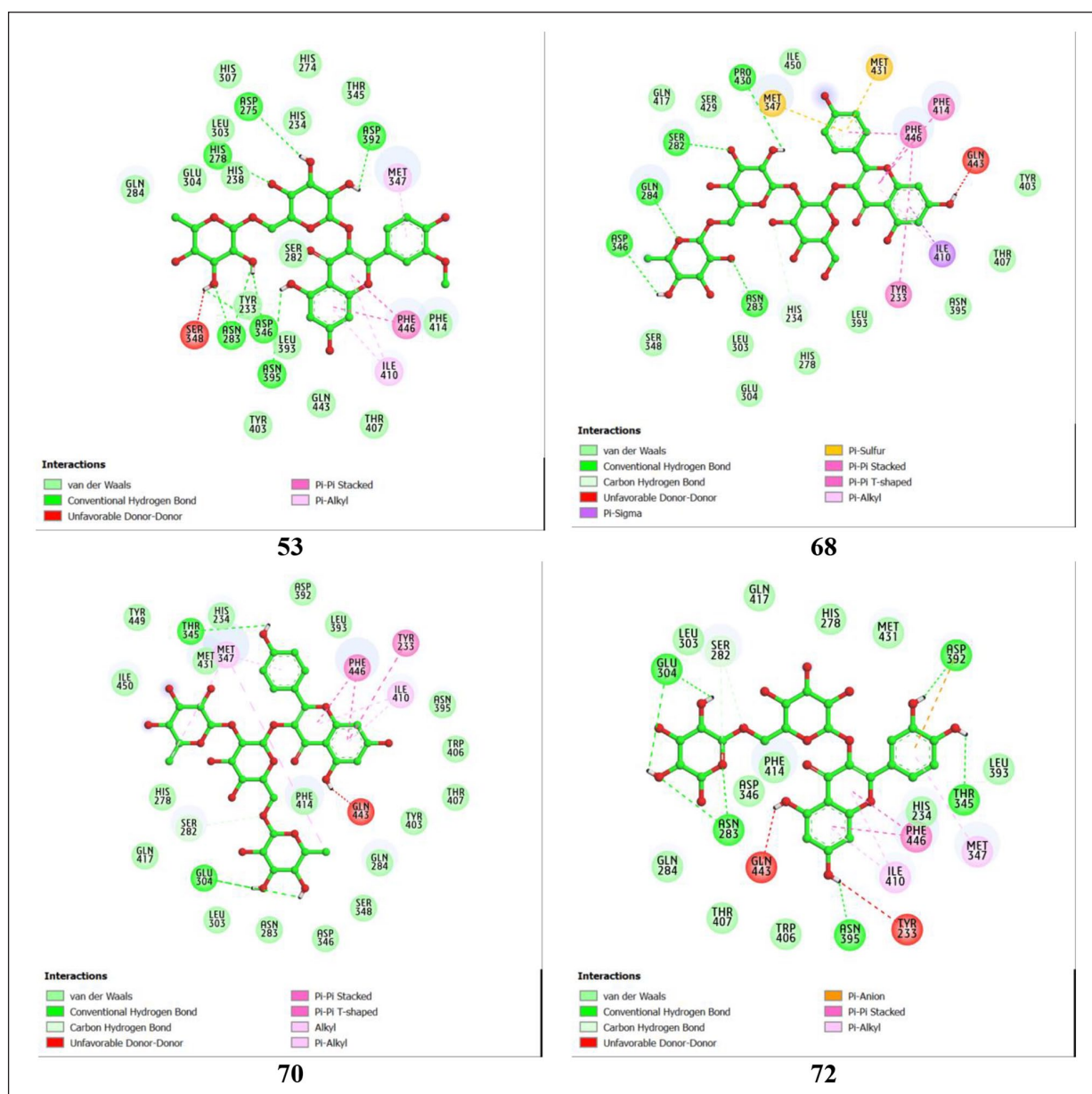


Figure 2. 2D interactions between amino acid residues of PDE4B protein (PDB ID 4KP6) and top-hit compounds.

hydrogen bonds significantly enhances the stability and binding affinity of the protein–ligand complexes. Compound 40 forms hydrogen bonds with Tyr233, Asn283, His278, Thr345, and His234. Compound 42 forms hydrogen bonds with Asn395, Met347, and Glu304. Compound 50 establishes hydrogen bonds with residues His278, Asp392, Asn283, Asp346, and Gln443. Compound 53 forms hydrogen bonds with residues Asn395, Asp346, Asn283, Asp275, Asp392, and His278. Hydrophobic interactions, including π -alkyl, π - π T-shaped, π - π stacked, π -sulfur, and π - σ interactions, are also observed in the complexes of these compounds with the PDE4B protein. Detailed interactions of compounds 40, 42, 44, 50, and 53 with the amino acid residues of the PDE4B protein are presented in Table 1.

Two kaempferol derivatives, compounds 68 and 70, and one quercetin derivative, compound 72, show similar binding affinities of -10.2 kcal/mol, -10.13 kcal/mol, and -10.1 kcal/mol, respectively. Compound 68 forms hydrogen

bonds with Asp346, Asn283, Gln284, Ser282, and Pro430, while compound 70 forms bonds with Thr345 and Glu304. Compound 72 establishes hydrogen bonds with five residues—Glu304, Asn283, Asn395, Thr345, and Asp392. Other interactions of compounds 68, 70, and 72 with the amino acid residues of the PDE4B protein are detailed in Table 1.

Overall, the compounds interact with key amino acid residues in PDE4B's catalytic domain such as a metal binding M pocket (His234, Asp346, Met347, Asp392), solvent-filled side pocket (Phe414, Ser282), and Q switch and P clamp pocket (Ile410, Asn395, Phe446, and Gln443) and, indicating their potential as PDE4B inhibitors.²⁹

MD simulation

To evaluate the stability and interactions of the protein–ligand complexes with PDE4B for the most promising

compounds ($\Delta G \leq 10$ kcal/mol), we analyzed the results of MD simulations. The RMSD values for the protein backbone and ligands are presented in Figure 3 and Supplemental Figure S1. Throughout the 200 ns simulation, the RMSD values of the protein in the complexes showed minor changes, staying below 0.3 nm with average values ranging from 0.1557 to 0.2375 nm, compared with 0.1671 nm for the apo-protein. The RMSD values for the proteins in the PDE4B-17, PDE4B-42, PDE4B-50, and PDE4B-70 complexes remained stable, showing minimal fluctuations around fixed points with no significant deviations. For the PDE4B-16 complex, a slight increase in protein backbone RMSD was observed, rising from approximately 0.15 nm at 55 ns to 0.23 nm at 60 ns, after which it stabilized for the remainder of the simulation. A similar trend was seen in the PDE4B-44 complex, where the RMSD increased modestly from 0.13 nm at 55 ns to 0.22 nm at 60 ns before reaching stability. Notably, the PDE4B-44 complex displayed minor structural adjustments during the early phases but achieved stability after 30 ns. The PDE4B-53 complex experienced fluctuations in protein backbone RMSD between 75 and 110 ns, after which it stabilized. In contrast, the PDE4B-68 complex showed an unusual spike in RMSD at 125 ns, remaining unstable through the end of the simulation. Meanwhile, the protein backbone RMSD of the PDE4B-72 complex remained unstable until around 100 ns, when it gradually began to stabilize.

Regarding ligand structure, the average RMSD values ranged from 0.1817 to 0.3627 nm. Among them, the ligand in the PDE4B-17 complex proved to be the most stable, with an average RMSD of just 0.1817 nm. In the PDE4B-16 complex, the ligand displayed a slight increase of approximately 0.1 nm at 20 ns but maintained stability afterward. The RMSD values for the ligands in the PDE4B-17, PDE4B-40, PDE4B-42, and PDE4B-44 complexes fluctuated around fixed points, showing no significant shifts. The ligand in the PDE4B-53 complex underwent considerable changes during the first 25 ns, yet its RMSD eventually stabilized for the remainder of the simulation. These observations highlight the resilience of the bound complexes, which retained their structural integrity despite internal thermal and dynamic fluctuations. In conclusion, the MD simulations strongly suggest that these protein–ligand complexes are stable, with the ligands firmly and consistently bound to the proteins.

The root mean square fluctuation (RMSF) measures the motion and flexibility of amino acid residues in a protein. Higher RMSF values indicate greater movement and flexibility, particularly at active sites, while extremely low RMSF values signify a stable and rigid active site. The RMSF profiles of the PDE4B complexes with the studied compounds, shown in Figure 4, highlight these dynamics. In the regions of amino acids 280–300 and 430–450, the PDE4B complexes with compounds 16, 17, 40, 42, 53, 70, and 72 exhibit lower RMSF values compared with the apo-protein structure, indicating stable binding in these areas. Conversely, the PDE4B-44 complex shows increased flexibility at both regions, and the PDE4B-50 and PDE4B-68 complexes exhibit significant flexibility at the 430–450

region. Fluctuations in other regions align with those of the apo-PDE4B protein. Notably, the regions 280–300 and 430–450 contain key residues involved in binding interactions, as reported in the “Molecular docking” section, demonstrating the significant potential for effective PDE4B inhibition by the compounds.

MM–GBSA binding free energy calculation

The MM–PBSA analysis was conducted to evaluate the binding affinities of the studied compounds and the reference inhibitor to the target protein PDE4B. The nonbonding energy, the more negative, indicates stronger ligand–protein interactions. The energies corresponding to the ligand–target complexes are presented in Table 2. The results indicate that the PDE4B complexes with the studied compounds have binding free energies ranging from -79.54 to -45.09 kcal/mol. It can be observed that compared with the reference inhibitor 1S1, all the compounds exhibit stronger binding free energies. This suggests that the most potent plant compounds show stronger binding affinities and increased stability with PDE4B.

Toxicity profiles

Toxicity prediction is a crucial step in drug development to protect human health by ensuring that new compounds are not harmful. This process saves time and costs, increases research efficiency, and minimizes risks for subsequent experimental studies. It also enhances research ethics by reducing the use of animals in testing.^{30,31} Thus, the ProTox 3.0 online tool was utilized in the current study to predict the toxicity of potential compounds through parameters such as LD_{50} , hepatotoxicity, neurotoxicity, nephrotoxicity, respiratory toxicity, and cardiotoxicity.²⁴ The results, recorded in Table 3, show that the predicted compounds have high LD_{50} values (≥ 5000 mg/kg) and low toxicity levels, indicating safety for oral administration. Specifically, compounds 16 and 17 were categorized with a toxicity level of 6, which is considered safe, while compounds 40, 42, 44, 50, 53, 68, 70, and 72 were classified at toxicity level 5. In addition, organ-specific toxicity analyses were conducted, revealing that hepatotoxicity and neurotoxicity of the compounds were predicted to be inactive. However, these compounds exhibited respiratory toxicity, suggesting they should not be used via inhalation. Compounds 16 and 17 were found to be active for cardiotoxicity but inactive for nephrotoxicity. Conversely, compounds 40, 42, 50, 53, 68, 70, and 72 showed the opposite predictions. Compound 44 was noted to be active for both cardiotoxicity and nephrotoxicity. These findings provide a foundation for the further experimental evaluation of the surveyed compounds in future studies.

Conclusion

In this study, a virtual screening method involving molecular docking and MD was conducted to identify novel PDE4B inhibitors and provide insights into the underlying

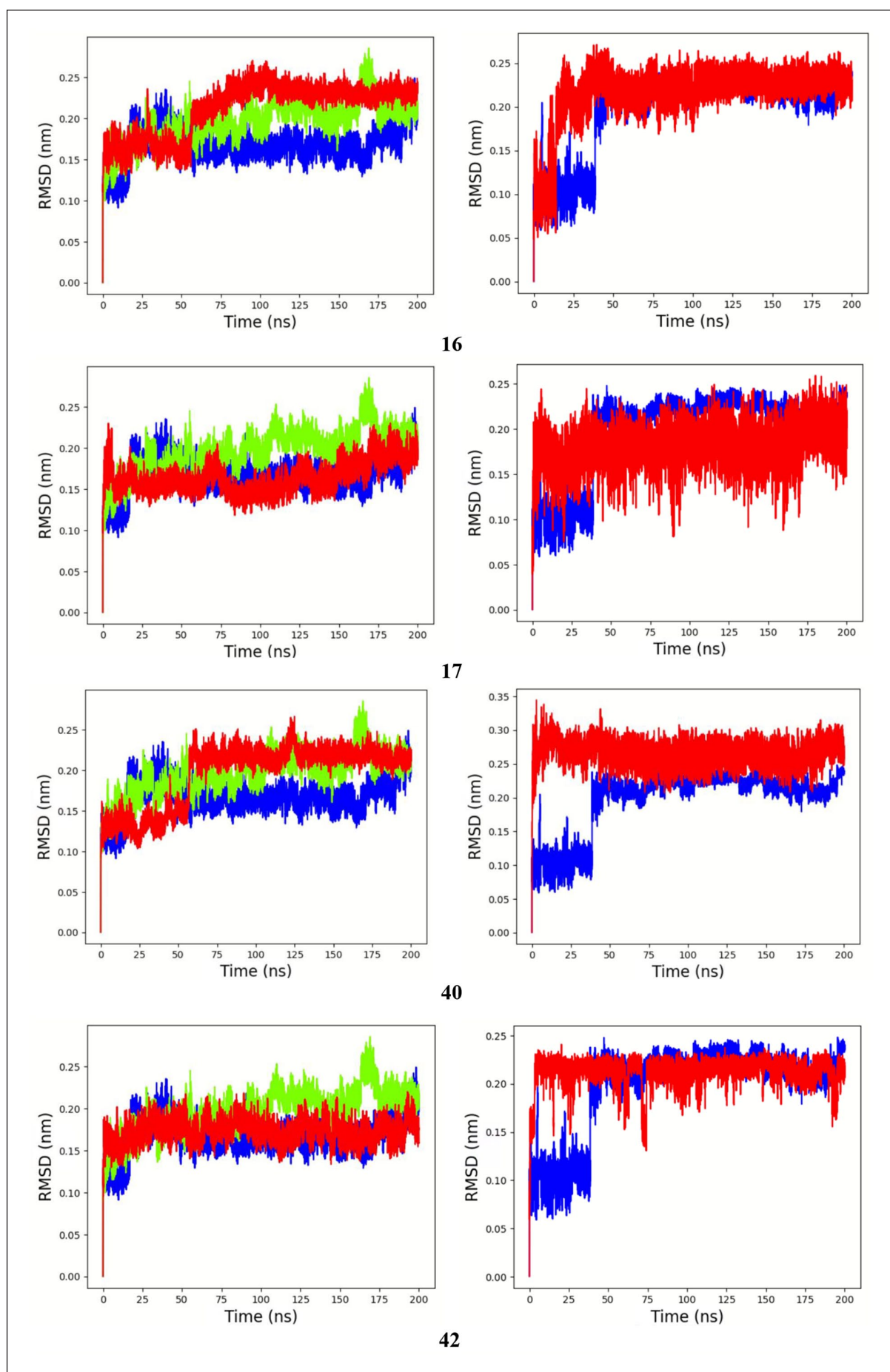


Figure 3. (Continued)

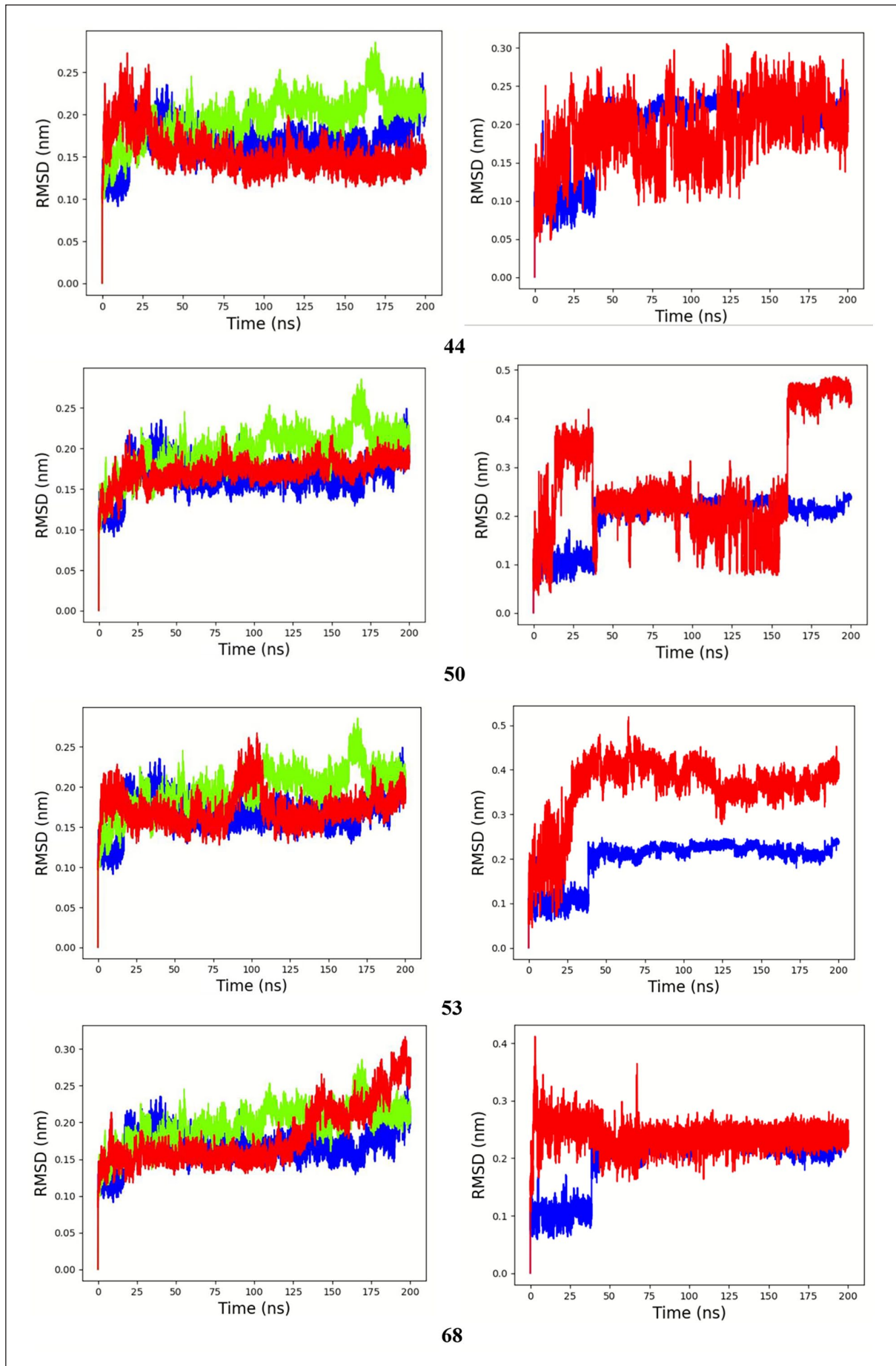


Figure 3. (Continued)

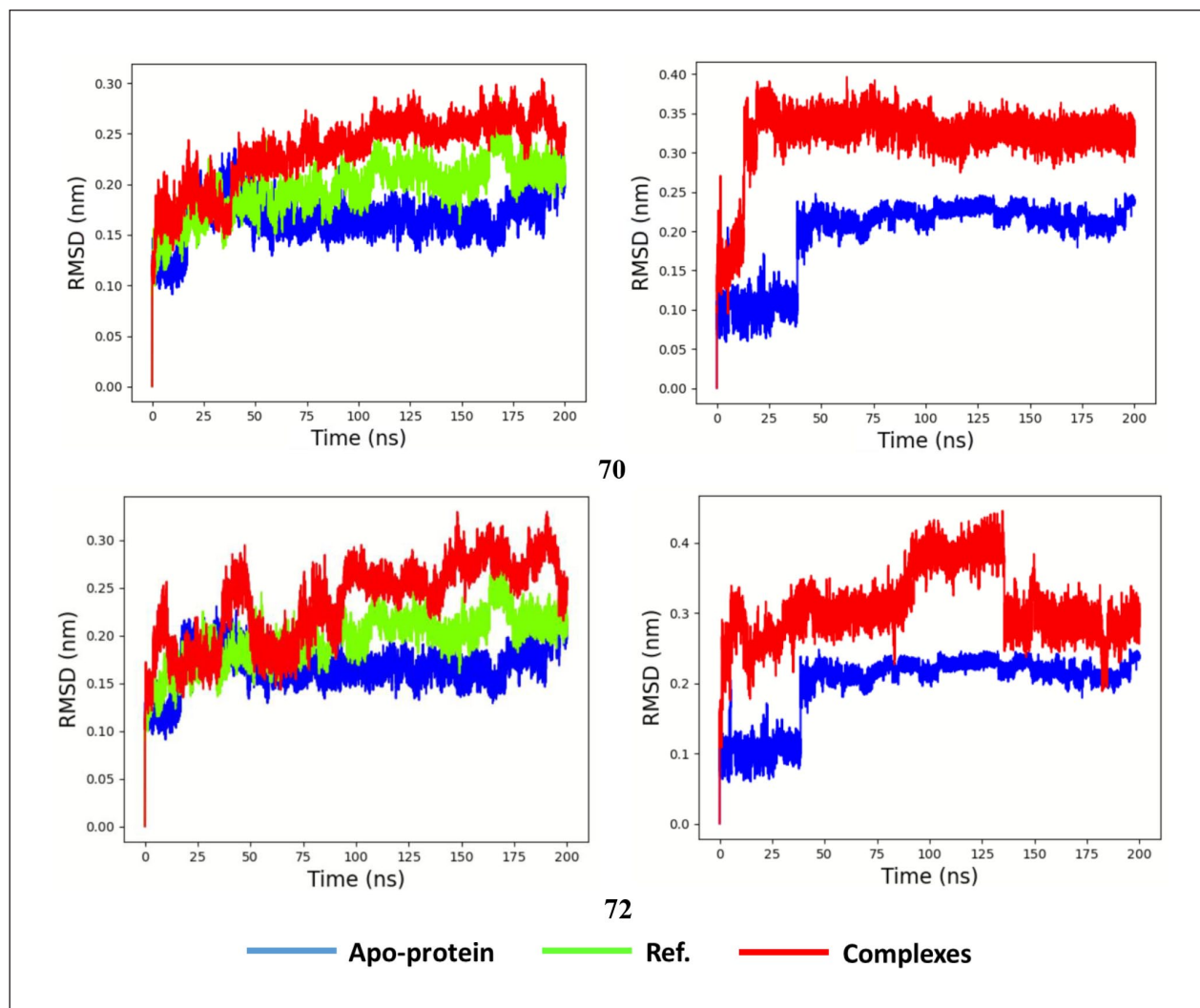


Figure 3. Root mean square deviation (RMSD) analysis of the backbone (right) and ligand (left) atoms of PDE4B complexes.

mechanisms of action of the identified potential compounds. As a result, the top 10 potential compounds, including *2 α -O-trans-p-coumaroyl-3 β ,19 α -dihydroxy-urs-12-en-28-oic acid*, *2 α -O-cis-p-coumaroyl-3 β ,19 α -dihydroxy-urs-12-en-28-oic acid*, *cyanidin-3-O-rutinoside*, *delphinidin-3-O-rutinoside*, *peonidin-3-O-rutinoside*, *rutin*, *isorhamnetin-3-O-rutinoside*, *kaempferol 3-O- α -L-rhamnopyranosyl-(1 \rightarrow 6)- β -D-glucopyranoside-7-O- β -D-glucopyranoside*, *Kaempferol 3-O- α -L-rhamnopyranosyl-(1 \rightarrow 6) [α -L-rhamnopyranosyl-(1 \rightarrow 2)]- β -D-glucopyranoside*, *quercetin 3-O- α -L-rhamnopyranosyl-(1 \rightarrow 6)- β -D-glucopyranoside*, demonstrated strong binding affinities

with PDE4B ($\Delta G \leq 10$ kcal/mol). Furthermore, MD simulations were performed to confirm the binding affinities and stability of these compounds in the active site of PDE4B. The binding free energies via MM-GBSA calculations showed that the surveyed compounds had stronger binding free energies than the reference inhibitor. In addition, regarding toxicity, the predicted compounds were all indicated to have safe toxicity levels; however, there were some considerations for use in subsequent stages. Overall, these results are significant for researchers in developing novel PDE4B receptor inhibitors for treating chronic inflammation.

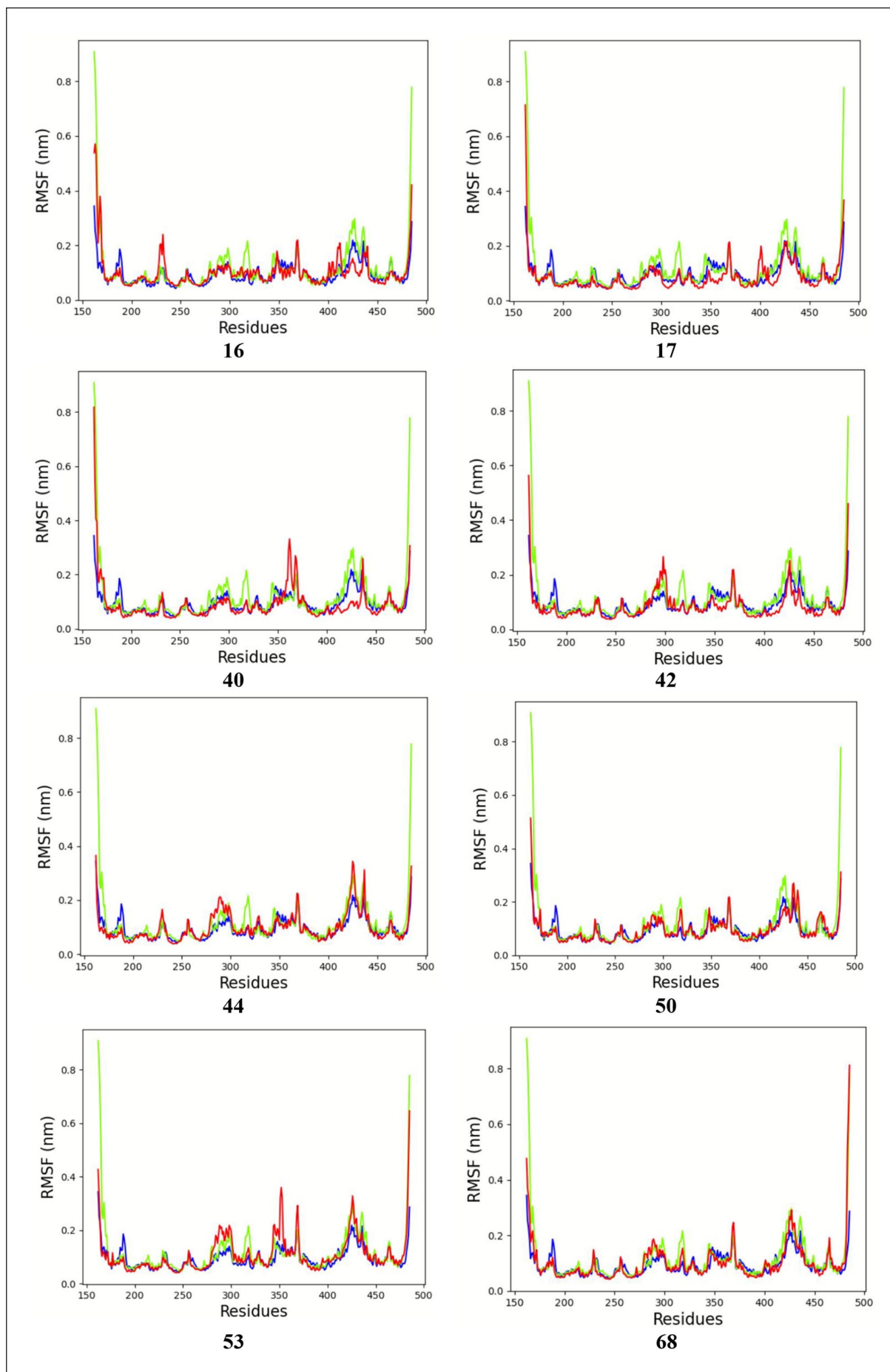


Figure 4. (Continued)

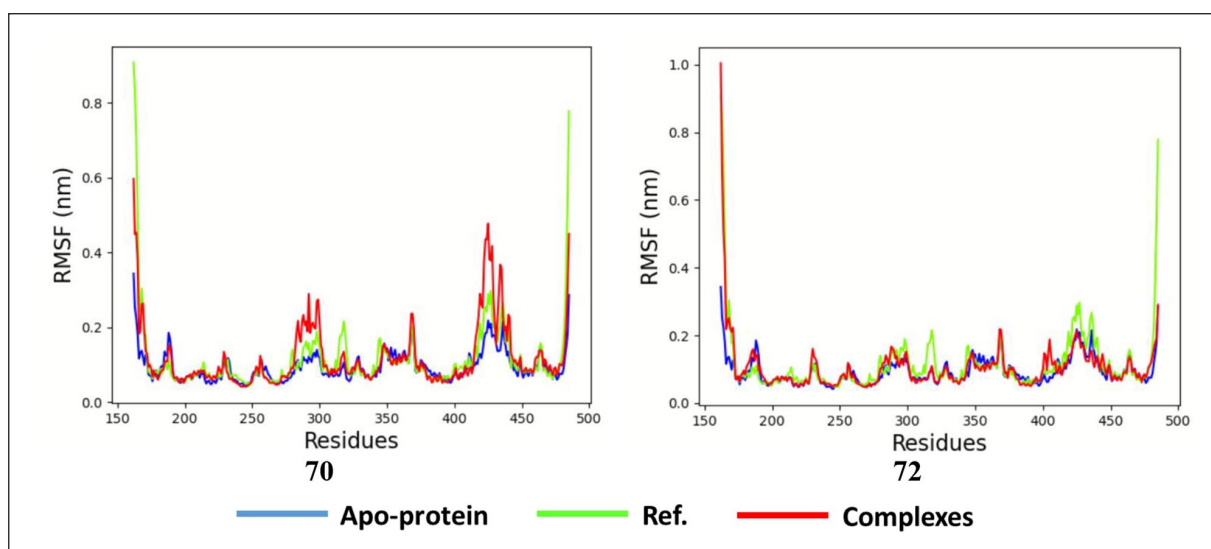


Figure 4. Root mean square fluctuation (RMSF) analysis of the backbone atoms of PDE4B and its complexes.

Table 2. The binding free energy in kcal.mol⁻¹ for the studied systems, determined via MM-GBSA calculations.

Energy component (kcal/mol)	16	17	40	42	44	50	53	68	70	72	ISI
VDWAALS	-73.51	-56.15	-60.31	-49.63	-65.72	-51.44	-59.82	-60.82	-66.64	-72.13	-44.34
EEL	329.49	314.76	295.65	289.71	323.92	-2.47	-1.57	-2.03	-5.92	-0.58	-0.78
E _{GB}	-304.80	-296.52	-285.36	-311.56	-306.81	14.10	15.55	17.22	21.68	18.35	9.43
E _{SURF}	-9.23	-7.18	-7.63	-8.06	-8.68	-6.07	-7.17	-7.22	-8.03	-8.78	-5.08
ΔG _{gas}	255.98	258.61	235.34	240.08	258.20	-53.91	-61.38	-62.86	-72.56	-72.71	-45.13
ΔG _{solv}	-314.03	-303.70	-292.99	-319.62	-315.50	8.03	8.38	10.00	13.66	9.57	4.35
ΔG _{total}	-58.05	-45.09	-57.65	-79.54	-57.29	-45.88	-53.00	-52.86	-58.91	-63.14	-40.78

Table 3. The oral toxicity prediction of the top-hit compounds.

Compound	Predicted LD ₅₀ (mg/kg)	Predicted Toxicity Class	Hepatotoxicity	Neurotoxicity	Nephrotoxicity	Respiratory toxicity	Cardiotoxicity
16	9960	6	Inactive	Inactive	Inactive	Active	Active
17	9960	6	Inactive	Inactive	Inactive	Active	Active
40	5000	5	Inactive	Inactive	Active	Active	Inactive
42	5000	5	Inactive	Inactive	Active	Active	Inactive
44	5000	5	Inactive	Inactive	Active	Active	Active
50	5000	5	Inactive	Inactive	Active	Active	Inactive
53	5000	5	Inactive	Inactive	Active	Active	Inactive
68	5000	5	Inactive	Inactive	Active	Active	Inactive
70	5000	5	Inactive	Inactive	Active	Active	Inactive
72	5000	5	Inactive	Inactive	Active	Active	Inactive

Author contributions

P.T.T. and N.X.H. supervised the project. P.T.T., N.X.H., and C.H.M.C. designed the project. C.H.M.C., N.T.T.G., and L.T.M.C. calculated and analyzed the data. P.T.T. and N.X.H. wrote the paper. All authors discussed and analyzed the results of the manuscript.

Declaration of conflicting interests

The author(s) declared no potential conflicts of interest with respect to the research, authorship, and/or publication of this article.

Funding

The author(s) received no financial support for the research, authorship, and/or publication of this article.

Ethical approval

Ethical approval is not applicable for the article.

Statement of human and animal rights

This article does not contain any studies with human or animal subjects.

Statement of informed consent

There are no human subjects in this article, and informed consent is not applicable.

ORCID iDs

Nguyen Xuan Ha  <https://orcid.org/0000-0002-8779-256X>

Phan Thi Thuy  <https://orcid.org/0000-0002-4571-5953>

Supplemental material

Supplemental material for this article is available online.

References

- Coussens LM and Werb Z. Inflammation and cancer. *Nature* 2002; 420(6917): 860–867.
- Su Y, Ding J, Yang F, et al. The regulatory role of PDE4B in the progression of inflammatory function study. *Front Pharmacol* 2022; 13: 982130.
- Dastidar SG, Rajagopal D and Ray A. Therapeutic benefit of PDE4 inhibitors in inflammatory diseases. *Curr Opin Investig Drugs* 2007; 8(5): 364–372.
- Tavares LP, Negreiros Lima GL, Lima KM, et al. Blame the signaling: role of cAMP for the resolution of inflammation. *Pharmacol Res* 2020; 159: 105030.
- Al-Nema M, Gaurav A and Lee VS. Docking based screening and molecular dynamics simulations to identify potential selective PDE4B inhibitor. *Heliyon* 2020; 6(9): e04856.
- Guariento S, Bruno O, Fossa P, et al. New insights into PDE4B inhibitor selectivity: CoMFA analyses and molecular docking studies. *Mo Divers* 2016; 20: 77–92.
- Sharma V and Wakode S. Structural insight into selective phosphodiesterase 4B inhibitors: pharmacophore-based virtual screening, docking, and molecular dynamics simulations. *J Biomol Struct Dyn* 2017; 35(6): 1339–1349.
- Kumar P, Kumar D and Rout SSS. Prinsepia utilis Royle: diversified and indigenous traditional uses of uncultivated multipurpose shrub. *Int J Mech Eng* 2021; 6: 974–5823.
- Chauhan K, Tripathi YC and Varshney VK. Prinsepia utilis Royle: a review on its traditional uses, phytochemistry, and biological activities. *Phytochem Lett* 2023; 55: 44–55.
- Kilidhar SB, Parthasarathy MR and Sharma P. Prinsepia, a lignan from stems of Prinsepia utilis. *Phytochemistry* 1982; 21(3): 796–797.
- Guan B, Peng CC, Zeng Q, et al. Cytotoxic pentacyclic triterpenoids from Prinsepia utilis. *Planta Medica* 2013; 79(05): 365–368.
- Thakur V, Guleria R and Singh R. Anti-inflammatory activity of Prinsepia utilis flower extract in Wistar rats. *Res J Pharmacognosy Phytochem* 2018; 10(4): 282–284.
- Chauhan K, Bhalla P, Chitme HR, et al. Exploring the therapeutic potential of Prinsepia utilis Royle seed oil: a comprehensive study on chemical composition, physicochemical properties, anti-inflammatory, and analgesic activities. *J Ethnopharmacol* 2024; 319: 117312.
- Shen W, Li SY, Pan YQ, et al. Prinsepia utilis Royle leaf extract: ameliorative effects on allergic inflammation and skin lesions in allergic contact dermatitis and polyphenolic profiling through UPLC–MS/MS coupled to chemometric analysis. *J Ethnopharmacol* 2023; 305: 116093.
- Halgren TA and MMFF VI. MMFF94s option for energy minimization studies. *J Comput Chem* 1999; 20(7): 720–729.
- Gewald R, Grunwald C and Egerland U. Discovery of triazines as potent, selective and orally active PDE4 inhibitors. *Bioorg Med Chem Lett* 2013; 23(15): 4308–4314.
- Trott O and Olson AJ. AutoDock Vina: improving the speed and accuracy of docking with a new scoring function, efficient optimization, and multithreading. *J Comput Chem* 2010; 31(2): 455–461.
- Eberhardt J, Santos-Martins D, Tillack AF, et al. AutoDock Vina 1.2. 0: new docking methods, expanded force field, and python bindings. *J Chem Inf Model* 2021; 61(8): 3891–3898.
- Van Der Spoel D, Lindahl E, Hess B, et al. GROMACS: fast, flexible, and free. *J Comput Chem* 2005; 26(16): 1701–1718.
- Frisch MJ, Trucks GW, Schlegel HB, et al. *Gaussian 09*. Wallingford, CT: Gaussian Inc, 2009.
- Sousa da Silva AW and Vranken WF. ACPYPE-antechamber python parser interface. *BMC Res Notes* 2012; 5: 367.
- Valdés-Tresanco MS, Valdés-Tresanco ME, Valiente PA, et al. gmx_MMPBSA: a new tool to perform end-state free energy calculations with GROMACS. *J Chem Theory Comput* 2021; 17(10): 6281–6291.
- Wang C, Greene DA, Xiao L, et al. Recent developments and applications of the MMPBSA method. *Front Mol Biosci* 2018; 4: 87.
- Banerjee P, Kemmler E, Dunkel M, et al. ProTox 3.0: a web-server for the prediction of toxicity of chemicals. *Nucleic Acids Res* 2024; 52: W513–W520.
- Ma DL, Chan DSH and Leung CH. Molecular docking for virtual screening of natural product databases. *Chem Sci* 2011; 2(9): 1656–1665.
- Le VTT, Hung HV, Ha NX, et al. Natural phosphodiesterase-4 inhibitors with potential anti-inflammatory activities from Millettia dielsiana. *Molecules* 2023; 28(21): 7253.
- Tran TH, Thang TD, Nguyen TH, et al. Essential oils from the trunks and leaves of Paramignya scandens (Griff.) Craib from Vietnam: phytochemical composition, in vitro α -amylase and tyrosinase inhibitory activities and in silico molecular docking studies. *Nat Prod Commun* 2023; 18(12): 1934578X231222383.
- Tran TH, Thuy PT, Thuan VT, et al. Chemical composition and antimicrobial activity of essential oil obtained from the rhizomes of Kaempferia champasakensis: in vitro and molecular docking studies. *J Essent Oil Bear Plants* 2023; 26(4): 958–969.
- Card GL, England BP, Suzuki Y, et al. Structural basis for the activity of drugs that inhibit phosphodiesterases. *Structure* 2004; 12(12): 2233–2247.
- Dearden JC. In silico prediction of drug toxicity. *J Comput Aided Mol Des* 2003; 17(2): 119–127.
- Patel CN, Kumar SP, Rawal RM, et al. A multiparametric organ toxicity predictor for drug discovery. *Toxicol Mech Methods* 2020; 30(3): 159–166.